


Infrared fixed point in the massless twelve-flavor SU(3) gauge-fermion system

Anna Hasenfratz^{*} and Curtis T. Peterson[†]

Department of Physics, University of Colorado, Boulder, Colorado 80309, USA

 (Received 15 March 2024; accepted 30 April 2024; published 10 June 2024)

We present strong numerical evidence for the existence of an infrared fixed point in the renormalization group flow of the SU(3) gauge-fermion system with twelve massless fermions in the fundamental representation. Our numerical simulations using nHYP-smearred staggered fermions with Pauli-Villars improvement do not exhibit any first-order bulk phase transition in the investigated parameter region. We utilize an infinite volume renormalization scheme based on the gradient flow transformation to determine the renormalization group β function. The gradient flow β function exhibits a zero at $g_{\text{GF}^*}^2 = 6.60(62)$, implying that the system is infrared conformal. We calculate the leading irrelevant critical exponent $\gamma_g^* = 0.199(32)$. Our prediction for γ_g^* is consistent with available literature at the 1-2 σ level.

DOI: [10.1103/PhysRevD.109.114507](https://doi.org/10.1103/PhysRevD.109.114507)

I. INTRODUCTION

The infrared properties of the SU(3) gauge-fermion system with $N_f = 12$ massless fundamental flavors has been studied extensively using a variety of analytical and numerical techniques. Such techniques include perturbation theory [1–6], use of the gap equation [7,8], functional renormalization group methods [9,10], conformal expansion [11], conformal bootstrap [12], the background field method [13], perturbative non-relativistic quantum chromodynamics [14], large- N expansion [15], and nonperturbative lattice simulations [16–39]. Investigations based on lattice simulations have utilized finite-volume step-scaling [16–25], Monte Carlo renormalization group methods [26,27], hadron mass and decay constant spectroscopy [29–37], and the Dirac eigenmode spectrum [38,39]. Many investigations suggest that the $N_f = 12$ system is infrared conformal,¹ though a minority of studies conclude that the system is confining with chiral symmetry breaking, or are inconclusive, as they find neither direct evidence of chiral symmetry breaking nor of an infrared fixed point.²

Most lattice studies are affected by the presence of a bulk first-order phase transition [41–46]. Such unphysical phase transitions are triggered by strong ultraviolet

fluctuations in the fermion sector that prevent lattice simulations from reaching deep into the infrared regime. Even when strong couplings are reached, lattice cutoff effects make it difficult to take the proper continuum limit, leading to inconsistent results between different lattice formulations. It is imperative to reduce the ultraviolet fluctuations that trigger first-order bulk phase transitions. Reference [47] suggested including unphysical heavy Pauli-Villars fields to achieve the necessary improvement. Lattice Pauli-Villars fields are similar to their continuum analogue—they have the same action as the fermions but possess bosonic statistics. Their mass is at the level of the cutoff. Therefore, they decouple in the infrared limit, while in the ultraviolet they compensate for cutoff effects introduced by the fermions. This idea has been tested in simulations of the SU(3) gauge-fermion system with ten massless fundamental Dirac fermions (flavors) and the SU(4) gauge-fermion system four massless fundamental and four massless two-index Dirac fermions [48,49]. Both studies extended the reach into the infrared regime significantly, and both present clear evidence for infrared conformality in those systems. See also Refs. [44,45] for an alternative proposal to remove unphysical bulk phase transitions.

In this work, we utilize Pauli-Villars (PV) improvement to study the infrared properties of the massless SU(3) gauge-fermion system with $N_f = 12$ fundamental flavors. We calculate the renormalization group (RG) β function, defined as the logarithmic derivative of the renormalized running coupling $g^2(\mu)$ with respect to an energy scale μ as

$$\beta(g^2) = \mu^2 \frac{dg^2(\mu)}{d\mu^2}. \quad (1)$$

^{*}anna.hasenfratz@colorado.edu

[†]curtis.peterson@colorado.edu

¹See Refs. [1–4,6–8,11,12,16–18,21,24–27,29,31,32,34–37,39].

²See Refs. [13,15,19,20,30,33,40].

Published by the American Physical Society under the terms of the Creative Commons Attribution 4.0 International license. Further distribution of this work must maintain attribution to the author(s) and the published article's title, journal citation, and DOI. Funded by SCOAP³.

If the running coupling captures the infrared properties of the system, the zeros of the β function signal fixed points. In a conformal system it is expected that the β function vanishes at some coupling $g_\star^2 \neq 0$, where the gauge coupling becomes irrelevant and the system is infrared conformal.

On the lattice, it is convenient to use gradient flow (GF) transformation [50–52] as a continuous smearing operation to define an infinite-volume renormalization scheme [28,53–57]. In the GF scheme, the renormalized coupling $g_{\text{GF}}^2(t)$ in infinite volume at flow time $t \propto 1/\mu^2$ is defined in terms of the Yang-Mills energy density $E(t)$ as

$$g_{\text{GF}}^2(t) \equiv \mathcal{N} \langle t^2 E(t) \rangle, \quad (2)$$

where $\mathcal{N} = 128\pi^2/(3N_c^2 - 3)$ is a constant chosen to match g_{MS}^2 at tree-level and $\langle E(t) \rangle$ is predicted using the plaquette or other small gauge loops, like the clover operator [51]. The corresponding RG β function is

$$\beta_{\text{GF}}(g_{\text{GF}}^2) \equiv -t \frac{dg_{\text{GF}}^2(t)}{dt}. \quad (3)$$

The running coupling and its RG β function are scheme dependent. The GF scheme is known to reproduce the universal perturbative 2-loop β function [58], but that alone does not guarantee that it is a good probe of infrared conformality [59]. However, the infrared properties of the gradient flow running coupling in Eq. (2) can be related to the nonperturbative Wilsonian renormalization group. The gradient flow transformation can be interpreted as a real-space renormalization group transformation and the expectation values of flowed local operators correspond to RG blocked operators [54,55]. The GF running coupling defined in Eq. (2) is a dimensionless renormalized quantity. If it has an overlap with the relevant coupling that emerges from the perturbative Gaussian fixed point, it tracks the renormalized trajectory [60]. At the same time, it can be expressed as a combination of loops of size $\lesssim \sqrt{8t}$. As long as the system does not cross a phase boundary, it is an analytic function of the bare gauge coupling. Wilsonian RG considerations then imply that the GF coupling corresponds to the relevant/leading-irrelevant scaling operator at the Gaussian/conformal fixed points in the continuum limit. While we cannot prove the above statements rigorously, they rely on the well established and widely studied Wilsonian renormalization group principles.

To calculate the infinite volume gradient flow β function $\beta_{\text{GF}}(g_{\text{GF}}^2)$ from finite-volume simulations, we utilize the continuous β function method (CBFM) proposed in Refs. [28,53,56] and deployed extensively in Refs. [48,49,61–64] to a variety of strongly-coupled gauge-fermion systems. In this paper we follow the steps described in [62,64] with additional extensions for improved error estimation. We discuss the continuous β function method and its implementation in further detail in Sec. III.

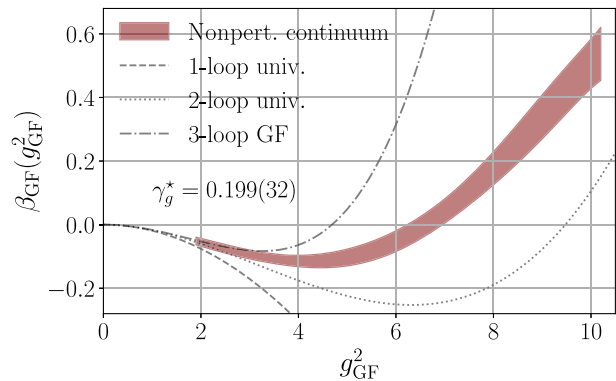


FIG. 1. Our continuum prediction for $\beta_{\text{GF}}(g_{\text{GF}}^2)$ as a function of g_{GF}^2 (maroon band) juxtaposed against the 1- (dashed), 2- (dotted) and 3-loop (dashed-dotted) gradient flow β function from perturbation theory [58]. The width of the maroon band indicates the error. Also given is our prediction for the leading irrelevant critical exponent at the IRFP, $\gamma_g^* = 0.199(32)$.

As a preview, we show our nonperturbative prediction for $\beta_{\text{GF}}(g_{\text{GF}}^2)$ as a function of g_{GF}^2 in Fig. 1. The predicted β function converges to the universal 1-/2-loop and 3-loop gradient flow perturbative β functions at small g_{GF}^2 [58]. Around $g_{\text{GF}\star}^2 = 6.60(62)$, the nonperturbative β function unambiguously exhibits an infrared fixed point. From the slope of $\beta_{\text{GF}}(g_{\text{GF}}^2)$ at $g_{\text{GF}\star}^2$, we calculate the leading irrelevant critical exponent $\gamma_g^* = 0.199(32)$ and find that it is consistent with the perturbative calculations of Refs. [4,6] at the 1σ level and the lattice calculation of Ref. [21] at the 2σ level. We control for systematic errors in the infinite volume extrapolation step of the CBFM using Bayesian model averaging. Additionally, our Pauli-Villars improved simulations offer tight control over systematics in the continuum extrapolation step of the CBFM.

This paper is laid out as follows. In Sec. II, we summarize details of our numerical simulations. In Sec. III, we review the continuous β function method and discuss our analysis. We explain our calculation of the leading irrelevant critical exponent in Sec. IV, and wrap up in Sec. V with conclusions.

II. NUMERICAL DETAILS

We simulate the massless twelve-flavor $\text{SU}(3)$ gauge-fermion system using an adjoint-plaquette gauge action with $\beta_F/\beta_A = -0.25$ ($\beta_F \equiv \beta_b$) and a massless ($am_f = 0.0$) nHYP-smearred staggered fermion action with four massive ($am_{\text{PV}} = 0.5$) Pauli-Villars (PV) fields per staggered fermion [47,65–67]. The “pions” of these PV fields have mass $am_{\text{PS}}^{(\text{PV})} \gtrsim 1.0^3$ and generate gauge loops in the effective gauge action with a size that decays

³PS = pseudoscalar.

TABLE I. The number of thermalized configurations analyzed at each bare coupling β_b and volume L/a . The configurations are separated by 10 MDTUs.

β_b	L/a				
	24	28	32	36	40
9.20	340	253	188	188	133
9.40	347	262	215	273	186
9.60	244	233	251	203	166
9.80	275	329	250	297	280
10.0	271	246	312	151	134
10.2	184	209	217	221	133
10.4	283	241	299	221	142
10.8	246	220	288	208	306
11.0	236	288	156	151	156
11.4	188	194	223	193	183
12.0	182	248	200	254	167
12.8	180	179	204	254	209
13.6	251	183	168	254	228
14.6	253	191	178	251	226

exponentially with $am_{\text{PS}}^{(\text{PV})}$ [47]. As long as the volume is much larger than $1/m_{\text{PS}}^{(\text{PV})}$ and $m_f \ll m_{\text{PS}}^{(\text{PV})}$ the PV fields decouple in the infrared. Their only effect is a modified, but local, gauge action. One of the goals of the present work is to illustrate the validity of this expectation.

We use antiperiodic boundary conditions in all four directions for both the staggered fermion fields and PV fields. Our numerical simulations are performed using the hybrid Monte Carlo algorithm [68] implemented in a modified version of the MILC library⁴ and the Quantum EXpressions (QEX) library [69].⁵ We set the molecular dynamics trajectory length to $\tau = 1.0$. Our configurations are separated by ten trajectories (ten molecular dynamics time units). We perform our simulations at fourteen bare gauge couplings ($9.20 \leq \beta_b \leq 14.6$) and five symmetric volumes ($24 \leq L/a \leq 40$). In Table I, we list the total number of thermalized configurations on each ensemble.

Our gradient flow measurements are performed using either the modified MILC or QEX libraries [69]. We flow our configurations using Wilson flow [51,52], integrating the gradient flow equations using the fourth-order Runge-Kutta algorithm discussed in Ref. [51] with time step $dt/a^2 = 0.02$ for $t/a^2 \leq 5.0$ and $dt/a^2 = 0.1$ for $t/a^2 > 5.0$. At each integration step, we measure the Yang-Mills energy density $E(t)$ using the Wilson (W) and clover (C) discretizations. In the rest of this paper, we refer to results based on Wilson flow and Wilson operator as WW, while we refer to results based on Wilson flow and clover

⁴The modified MILC library can be found at https://github.com/daschaich/KS_nHYP_FA.

⁵Our fork of QEX can be found at <https://github.com/cpterson/qex>.

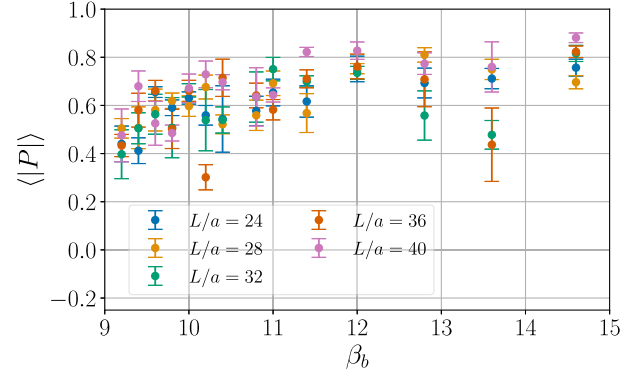


FIG. 2. The gradient-flow Polyakov loop expectation value at flow time $8t/a^2 \approx (L/2a)^2$ versus the bare gauge coupling β_b on each volume in Table I. The absolute value of the Polyakov loop is shown by colored error bars: $L/a = 24$ (blue), 28 (yellow), 32 (green), 36 (orange), and 40 (pink). The Polyakov loop is normalized to unity.

operator as WC. Our data for the Yang-Mills energy density $E(t)$ from the Wilson and clover operator are available at Ref. [70].

In Fig. 2 we plot the expectation value of the magnitude of the gradient-flow Polyakov loop $|P|$ at $8t/a^2 \approx (L/2a)^2$ against the bare gauge coupling β_b for all ensembles in Table I. The Polyakov loop is normalized to unity. Errors are estimated using the “ Γ -method” technique implemented by the PYERRORS package [71–74]; however, they are likely underestimated. Nonetheless, the Polyakov loop suggests that the system is not confining in the range of couplings and volumes that we use in the present study.

III. NONPERTURBATIVE β FUNCTION

We measure the gradient flow coupling in finite volume in terms of the Yang-Mills energy density $E(t)$ as

$$g_{\text{GF}}^2(t; L, g_0^2) \equiv \frac{\mathcal{N}}{1 + \delta(t, L)} \langle t^2 E(t) \rangle, \quad (4)$$

where $\delta(t, L)$ corrects for gauge zero modes [75]. From $g_{\text{GF}}^2(t; L, g_0^2)$, we calculate the gradient flow β function in finite volume as

$$\beta_{\text{GF}}(t; L, g_0^2) \equiv -t \frac{d}{dt} g_{\text{GF}}^2(t; L, g_0^2), \quad (5)$$

where we discretize d/dt with a 5-point stencil. The autocorrelation time for $g_{\text{GF}}^2(t; L, g_0^2)$ and $\beta_{\text{GF}}(t; L, g_0^2)$ is typically between 20–80 molecular dynamics time units (MDTUs), with occasional jumps to 120–200 MDTUs.

To extract the continuum $\beta_{\text{GF}}(g_{\text{GF}}^2)$ as a function of g_{GF}^2 , we follow the CBFM procedure outlined in Refs. [62,64].

- (1) Take the infinite volume limit by independently extrapolating both $g_{\text{GF}}^2(t; L, g_0^2)$ and $\beta_{\text{GF}}(t; L, g_0^2)$ linearly in $(a/L)^4 \rightarrow 0$ at fixed t/a^2 and β_b .
- (2) Interpolate $\beta_{\text{GF}}(t; g_0^2)$ in $g_{\text{GF}}^2(t; g_0^2)$ at fixed t/a^2 .
- (3) Take the continuum limit by extrapolating $\beta_{\text{GF}}(t; g_0^2)$ linearly in $a^2/t \rightarrow 0$ at fixed $g_{\text{GF}}^2(t)$.

Correlated uncertainties are propagated throughout our analysis using the automatic error propagation tools provided by the `gvar` library [76]. Fits are performed using the `SwissFit` library, which integrates directly with `gvar` [77]. The steps of the CBFM are detailed in the rest of this section.

A. Infinite volume extrapolation

Because the Yang-Mills energy density is a dimension-4 operator, leading finite-volume corrections to $g_{\text{GF}}^2(t; L, g_0^2)$ and $\beta_{\text{GF}}(t; L, g_0^2)$ are expected to be $\mathcal{O}(t^2/L^4)$. Therefore, we extrapolate both $g_{\text{GF}}^2(t; L, g_0^2)$ and $\beta_{\text{GF}}(t; L, g_0^2)$ to $a/L \rightarrow 0$ by independently fitting them to the ansatz,

$$\text{FV}(L/a) = k_1(a/L)^4 + k_2, \quad (6)$$

at fixed t/a^2 and β_b . This analysis strategy was first outlined in Ref. [64] and subsequently applied in Refs. [62,63]. Alternative methods are discussed in Refs. [28,53,56,61].

We account for the systematic uncertainty that is associated with choosing a particular subset of volumes for the infinite volume extrapolation using Bayesian model averaging [78–80]. We do so by first fitting over all possible subsets of volumes $L/a \in \{24, 28, 32, 36, 40\}$ with at least three volumes in each subset η . We calculate the model weight w_η for a particular subset η as

$$w_\eta \propto \exp\left[-\frac{1}{2}(\chi_\eta^2 + 2d_\eta)\right], \quad (7)$$

where χ_η^2 is the χ^2 statistic of fit η and d_η is the number of data points *not* included in fit η from the full set of volumes $\{24, 28, 32, 36, 40\}$. Denoting the mean of k_i from fit η as $\bar{k}_i^{(\eta)}$, our model-averaged prediction for the mean \bar{k}_i of k_i is

$$\bar{k}_i = \sum_\eta \bar{k}_i^{(\eta)} w_\eta, \quad (8)$$

where the weights w_η have been normalized such that $\sum_\eta w_\eta = 1$. The covariance C_{ij} of our model-averaged prediction for $\{k_i\}_{i=1,2}$ is

$$C_{ij} = \sum_\eta C_{ij}^{(\eta)} w_\eta + \sum_\eta \bar{k}_i^{(\eta)} \bar{k}_j^{(\eta)} w_\eta - \bar{k}_i \bar{k}_j, \quad (9)$$

where $C_{ij}^{(\eta)}$ is the covariance of $\{k_i^{(\eta)}\}_{i=1,2}$ from fit η .

In Figs. 3 and 4, we show the result of our model-averaged infinite volume extrapolation for the W and C discretization of $E(t)$, respectively, over a range of flow times $2.5 \leq t/a^2 \leq 6.0$ (different colors). The left panels of Figs. 3 and 4 show our infinite extrapolation of $g_{\text{GF}}^2(t; L, g_0^2)$, while the right panels show our infinite volume extrapolation of $\beta_{\text{GF}}(t; L, g_0^2)$. The bare gauge couplings that we chose for these plots are in the vicinity where the continuum β function predicts an infrared fixed point (IRFP). For all three bare gauge couplings shown in Figs. 3 and 4, the model average is dominated by subsets containing $L/a \in \{28, 32, 36, 40\}$, as $L/a = 24$ often deviates from the linear trend in a^4/L^4 , particularly as the flow time increases. This is reflected in the model average, as fits including $L/a = 24$ possess small model weights w_η and contribute negligibly to the model average.

B. Intermediate interpolation

The continuum limit $a^2/t \rightarrow 0$ of $\beta_{\text{GF}}(t; g_0^2)$ is taken at fixed g_{GF}^2 . We predict pairs $(t/a^2, \beta_{\text{GF}}(t; g_0^2))$ at a set of fixed g_{GF}^2 for the continuum extrapolation by interpolating $\beta_{\text{GF}}(t; g_0^2)$ in $g_{\text{GF}}^2(t; g_0^2)$ at fixed t/a^2 using the ansatz,

$$\mathcal{I}_N(g_{\text{GF}}^2) = g_{\text{GF}}^4 \sum_{i=0}^{N-1} p_n g_{\text{GF}}^{2n}. \quad (10)$$

At each t/a^2 , we account for the uncertainty in $g_{\text{GF}}^2(t; g_0^2)$ by including the mean and covariance of $g_{\text{GF}}^2(t; g_0^2)$ as a Gaussian prior. We also set a Gaussian prior on each coefficient p_n with zero mean and a width of 0.1, which helps stabilize the fit. We choose $N = 4$, as it is the lowest value of N that fits the data well. In Fig. 5, we show the result of our interpolation for the W operator (top panel) and the C operator (bottom panel) for several flow time values in the range $2.5 \leq t/a^2 \leq 6.0$ (different colors). The fits that enter our continuum extrapolation have p-values in the 83%–98% range. This could indicate that we are either overfitting or the errors in our data are overestimated. Reducing the order makes each interpolation significantly worse, as interpolations with $N \leq 3$ are unable to accommodate the varying curvature at weak/strong coupling. Therefore, use $N = 4$ for our central analysis. We will discuss the systematic effect that is associated with the order N in our estimate of $g_{\text{GF}\star}^2$ and γ_g^\star in Sec. IV.

C. Continuum extrapolation

The final step is the continuum ($a^2/t \rightarrow 0$) limit over a set of fixed g_{GF}^2 that predicts $\beta_{\text{GF}}(g_{\text{GF}}^2)$ as a function of g_{GF}^2 . The range of $[t_{\text{min}}/a^2, t_{\text{max}}/a^2]$ used in the continuum extrapolation must be chosen with care. The value of t_{min}/a^2 must be large enough for the RG flow to reach the renormalized trajectory. Once this is the case,

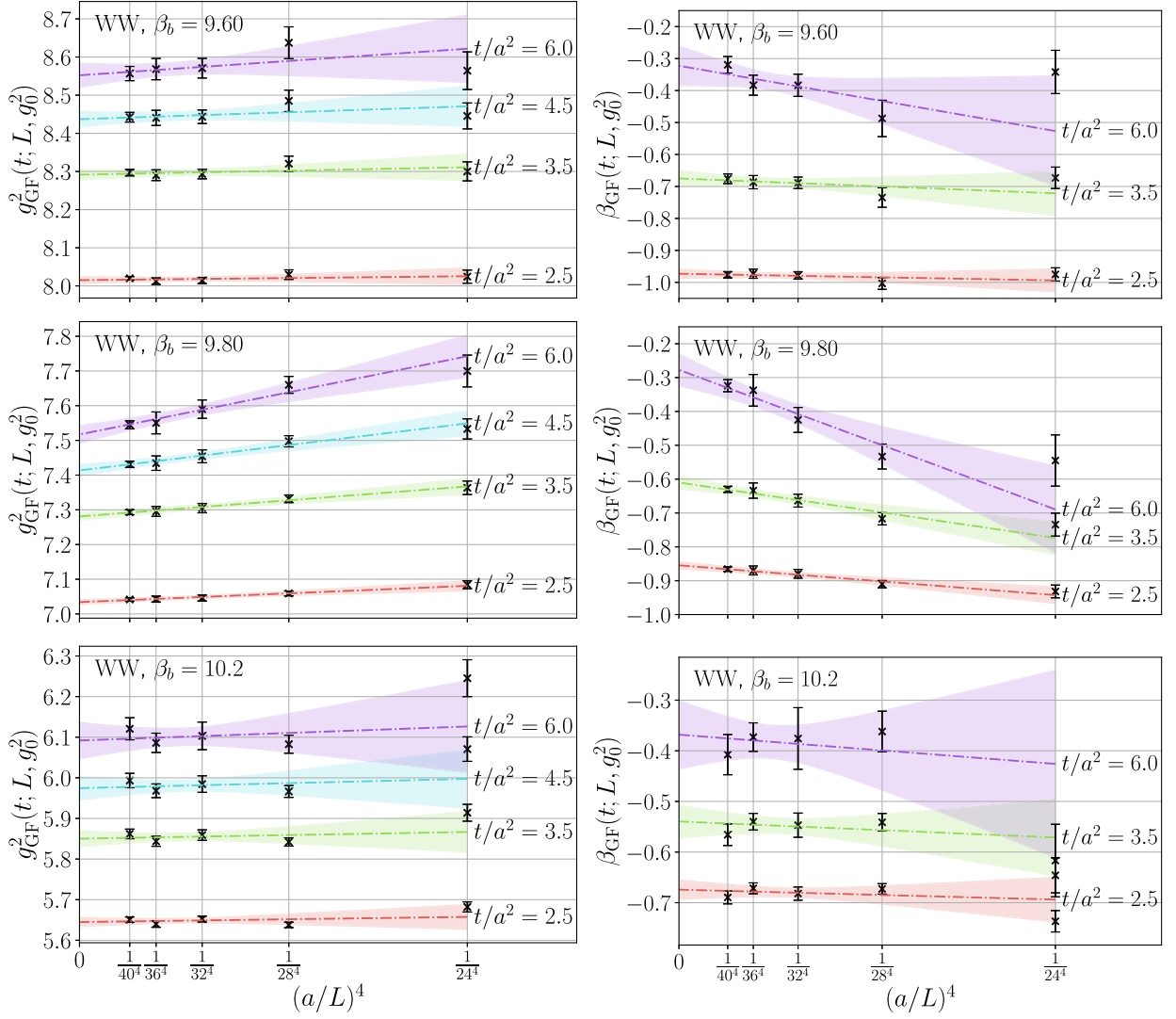


FIG. 3. Result of our infinite volume extrapolation of $g_{\text{GF}}^2(t; L, g_0^2)$ (left panels) and $\beta_{\text{GF}}(t; L, g_0^2)$ (right panels) for the Wilson (W) operator at $\beta_b = 9.60$ (top panels), 9.80 (middle panels), and 10.2 (bottom panels). Black (\times) markers with error bars are the data included in our extrapolation. Extrapolations with errors that are predicted from Bayesian model averaging are indicated by multicolored bands at $t/a^2 = 2.5$ (red), 3.5 (light green), 4.5 (cyan), and 6.0 (light purple). We do not show the infinite volume extrapolation of $\beta_{\text{GF}}(t; L, g_0^2)$ at $t/a^2 = 4.5$ for visualization purposes.

finite-cutoff effects are $\mathcal{O}(a^2/t)$. In practice, one can identify when t_{\min}/a^2 is close enough to the renormalized trajectory by the overlap between the continuum prediction for $\beta_{\text{GF}}(g_{\text{GF}}^2)$ from both operators. Because finite-volume effects are expected to be $\mathcal{O}(t^2/L^4)$, t_{\max}/a^2 must be chosen such $t/a^2 < t_{\max}/a^2$ has a reliable infinite volume extrapolation. Ideally, we would apply Bayesian model averaging to the continuum extrapolation to automatically account for systematic effect that is associated with making a particular choice in $[t_{\min}/a^2, t_{\max}/a^2]$. However, at this point in the analysis, we no longer have access to the full covariance matrix, which means that we no longer have access to a reliable estimate of the model weights. To estimate the error in our continuum extrapolation, we use

the half-difference of the prediction from the continuum extrapolation performed at $\pm 1\sigma$. This approach was also taken in Ref. [62].

Figure 6 shows examples of the continuum extrapolation performed in the range $2.0 \leq g_{\text{GF}}^2 \leq 6.0$ (different colors) using $[t_{\min}/a^2, t_{\max}/a^2] = [3.5, 6.0]$. For $t/a^2 \lesssim 3.5$, $\beta(t; g_0^2)$ has a slight curvature in a^2/t , indicating emerging higher-order cutoff effects for both the W and C operator. For $t/a^2 \gtrsim 6.0$, the data begins to deviate from a linear trend in a^2/t , indicating that the infinite volume extrapolation is getting unreliable. Our choice of $[t_{\min}/a^2, t_{\max}/a^2] = [3.5, 6.0]$ avoids both of these two regimes. In Sec. IV, we discuss the sensitivity of our prediction for $g_{\text{GF}\star}^2$ and γ_g^* to our choice of $t_{\min}/a^2, t_{\max}/a^2$.

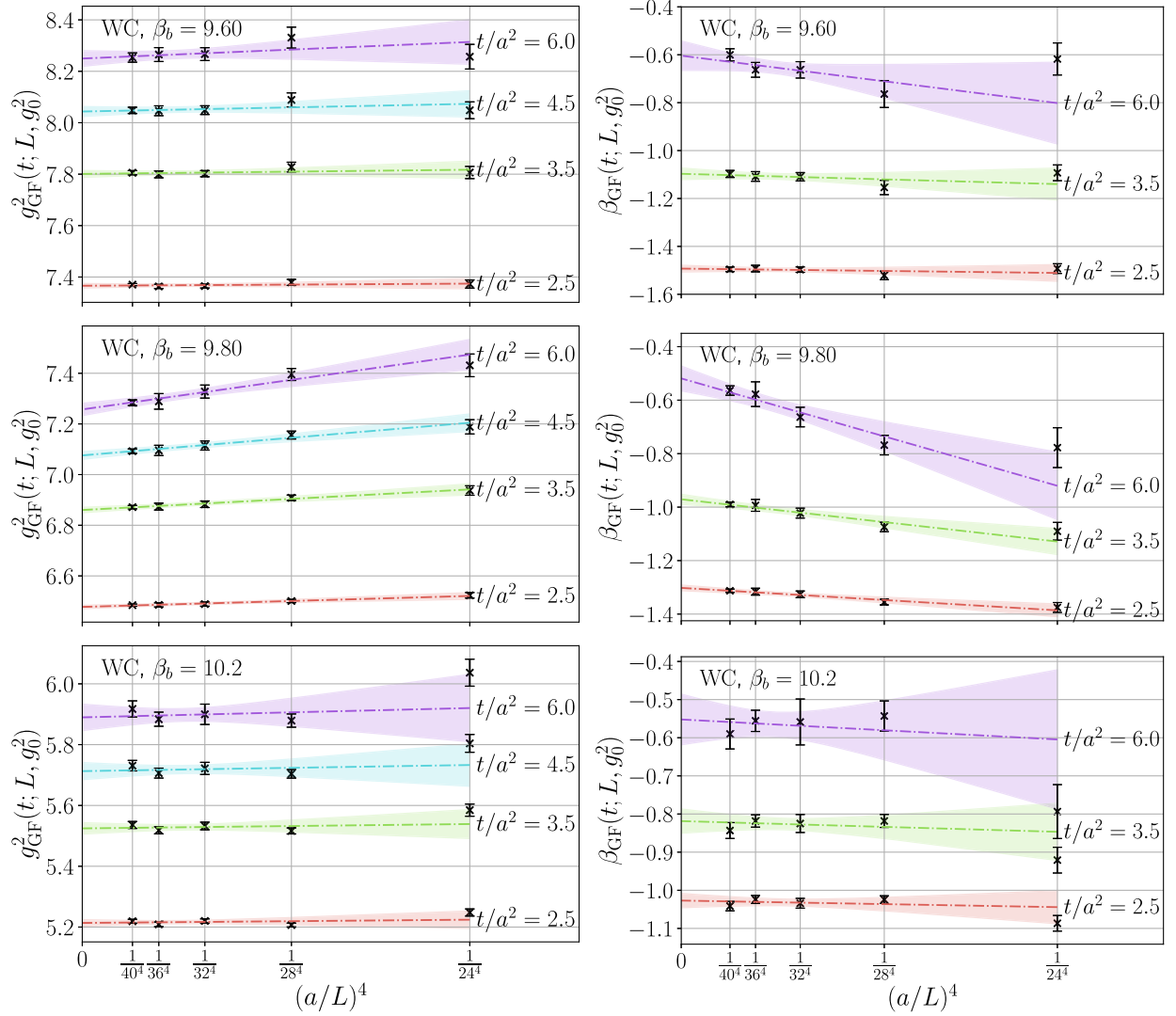


FIG. 4. Result of our infinite volume extrapolation of $g_{\text{GF}}^2(t; L, g_0^2)$ (left panels) and $\beta_{\text{GF}}(t; L, g_0^2)$ (right panels) for the clover (C) operator at $\beta_b = 9.60$ (top panels), 9.80 (middle panels) and 10.2 (bottom panels). Black (\times) markers with error bars are the data included in our extrapolation. Extrapolations with errors that are predicted from Bayesian model averaging are indicated by multicolored bands at $t/a^2 = 2.5$ (red), 3.5 (light green), 4.5 (cyan), and 6.0 (light purple). We do not show the infinite volume extrapolation of $\beta_{\text{GF}}(t; L, g_0^2)$ at $t/a^2 = 4.5$ for visualization purposes.

We show our prediction for the continuum $\beta_{\text{GF}}(g_{\text{GF}}^2)$ in Fig. 7 from the WW (gold band) and WC (maroon band) combination. The continuum predictions from both operators are consistent with one another across the entire range of investigated renormalized couplings g_{GF}^2 . At small g_{GF}^2 , the continuum $\beta_{\text{GF}}(g_{\text{GF}}^2)$ appears to converge to the 1-, 2-, and 3-loop perturbative gradient flow β function [58]. At $g_{\text{GF}\star}^2 \approx 6.60$, our continuum β function predicts an infrared fixed point. The location of the fixed point is slightly below the predicted IRFP from the step-scaling calculation of Ref. [21]. Note that, because the calculation in Ref. [21] was done in a different gradient-flow-based renormalization scheme, the predicted $g_{\text{GF}\star}^2$ values do not have to agree. Our final result for $\beta_{\text{GF}}(g_{\text{GF}}^2)$ from both operators is provided as an ASCII file.

IV. THE IRFP AND ITS LEADING IRRELEVANT CRITICAL EXPONENT

In the vicinity of the RG fixed point $g_{\text{GF}\star}^2$,

$$\beta(g_{\text{GF}}^2) \approx \frac{\gamma_g^\star}{2} (g_{\text{GF}}^2 - g_{\text{GF}\star}^2), \quad g_{\text{GF}}^2 \rightarrow g_{\text{GF}\star}^2, \quad (11)$$

where γ_g^\star is the universal critical exponent of the irrelevant gauge coupling. The factor of 1/2 is chosen to match the convention of Refs. [6,21]. We estimate $g_{\text{GF}\star}^2$ and γ_g^\star via the following procedure.

- (1) Interpolate the central value of $\beta(g_{\text{GF}}^2)$ and the central value of $\beta(g_{\text{GF}}^2) \pm 1\sigma$ in g_{GF}^2 using a monotonic spline.

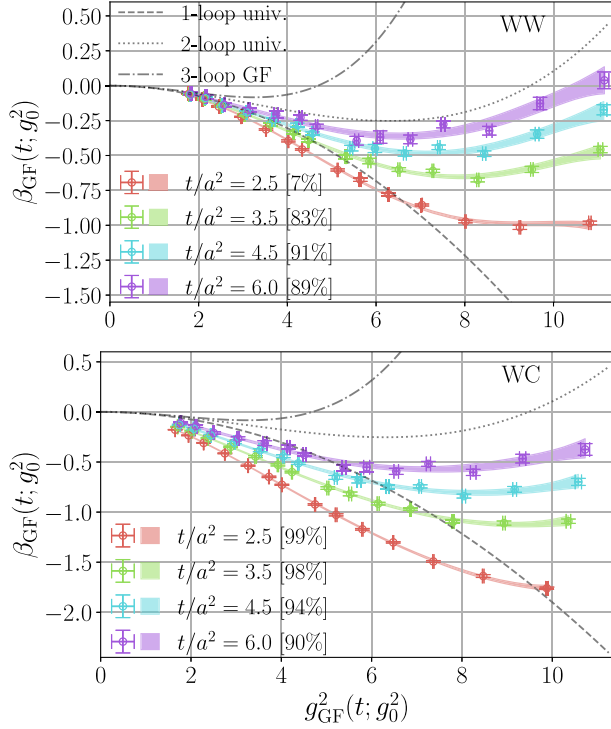


FIG. 5. Illustration of our interpolation of $\beta_{\text{GF}}(t; g_0^2)$ in $\beta_{\text{GF}}(t; g_0^2)$ for the Wilson operator (top panel) and clover operator (bottom panel). Interpolations at fixed t/a^2 are indicated by colored bands, with $t/a^2 = 2.5$ (red), 3.5 (light green), 4.5 (cyan), and 6.0 (light purple). The width of the band indicates the error. The data contributing to each interpolation are indicated by an open circular marker with both x- and y-errors. We compare our interpolation against the continuum 1- (dashed), 2- (dotted), and 3-loop (dashed-dotted) gradient flow β function from perturbation theory [58].

- (2) Estimate the central value of $g_{\text{GF}\star}^2$ from the root of the spline interpolation of $\beta(g_{\text{GF}}^2)$ in g_{GF}^2 .
- (3) Estimate the central value of γ_g^* from the derivative of the spline at $g_{\text{GF}\star}^2$.
- (4) Repeat steps (2)–(3) with a spline interpolation of $\beta(g_{\text{GF}}^2) \pm 1\sigma$ in g_{GF}^2 .
- (5) Estimate the error in $g_{\text{GF}\star}^2$ and γ_g^* from the half difference of their predictions from the interpolations in step (4).

Steps (1)–(5) yield $g_{\text{GF}\star}^2 = 6.69(35), 6.60(36)$ and $\gamma_g^* = 0.206(19), 0.199(18)$ for WW and WC, respectively. In Fig. 8 we look at how the continuum limit predictions for $g_{\text{GF}\star}^2$ (top panels) and γ_g^* (bottom panels) vary with our choice of t_{min}/a^2 (x-axes) and t_{max}/a^2 (different colors) for the W (left panels) and C (right panels) operators. The central values for both quantities and both operators are stable; they vary well within error. The stability in t_{min}/a^2 is attributed to the linearity of the continuum extrapolation over a wide range of a^2/t , while the stability in t_{max}/a^2 is likely attributed to our control over the infinite volume extrapolation.

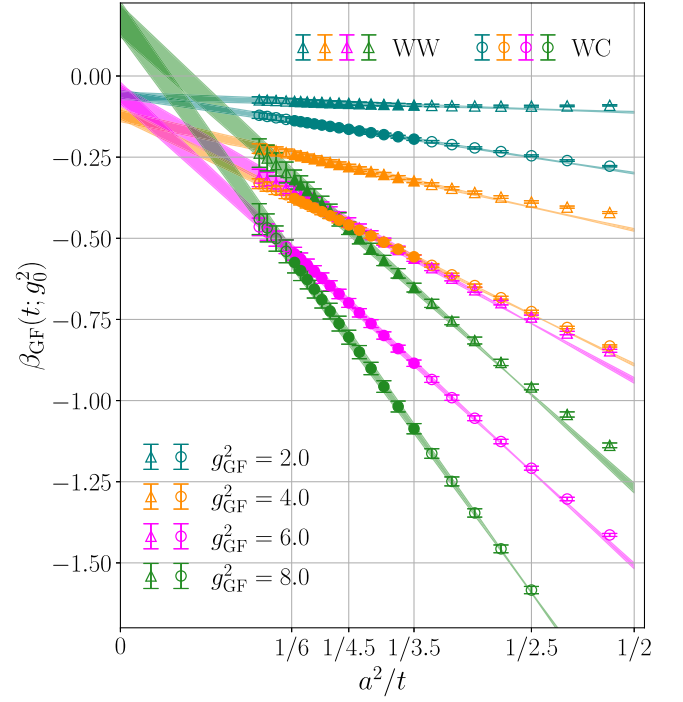


FIG. 6. Illustration of our continuum extrapolation of $\beta_{\text{GF}}(t; g_0^2)$ at fixed $g_{\text{GF}}^2 = 2.0$ (teal), 4.0 (dark orange), 6.0 (magenta), and 8.0 (forest green). Data contributing to our extrapolation with the W operator are shown as error bars with triangular markers and the C operator are shown as error bars with circular markers. Our extrapolations are shown as colored bands, where the error is indicated by the width of the band.

We take the result for γ_g^* from the WC combination with the value for $[t_{\text{min}}/a^2, t_{\text{max}}/a^2] = [3.5, 6.0]$ from Sec. V as our central result. We estimate additional systematic errors by varying our analysis as follows.

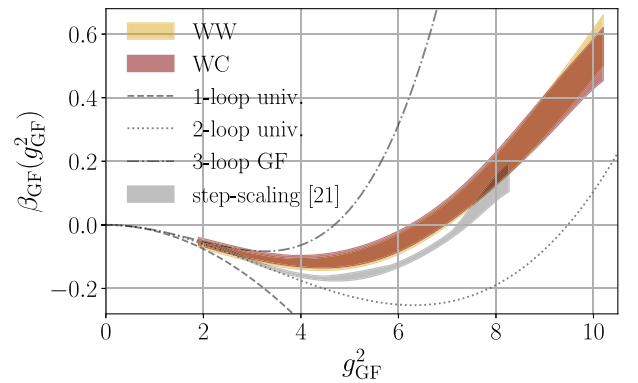


FIG. 7. Our continuum prediction for $\beta_{\text{GF}}(g_{\text{GF}}^2)$ as a function of g_{GF}^2 for the W operator (gold band) and C operator (maroon band). The width of the band indicates the error. The nonperturbative results are juxtaposed against the 1- (dashed), 2- (dotted), and 3-loop (dashed-dotted) gradient flow β function from perturbation theory [58]. Also shown is the step-scaling β function in the $c = 0.25$ scheme from Ref. [21] as a gray band.

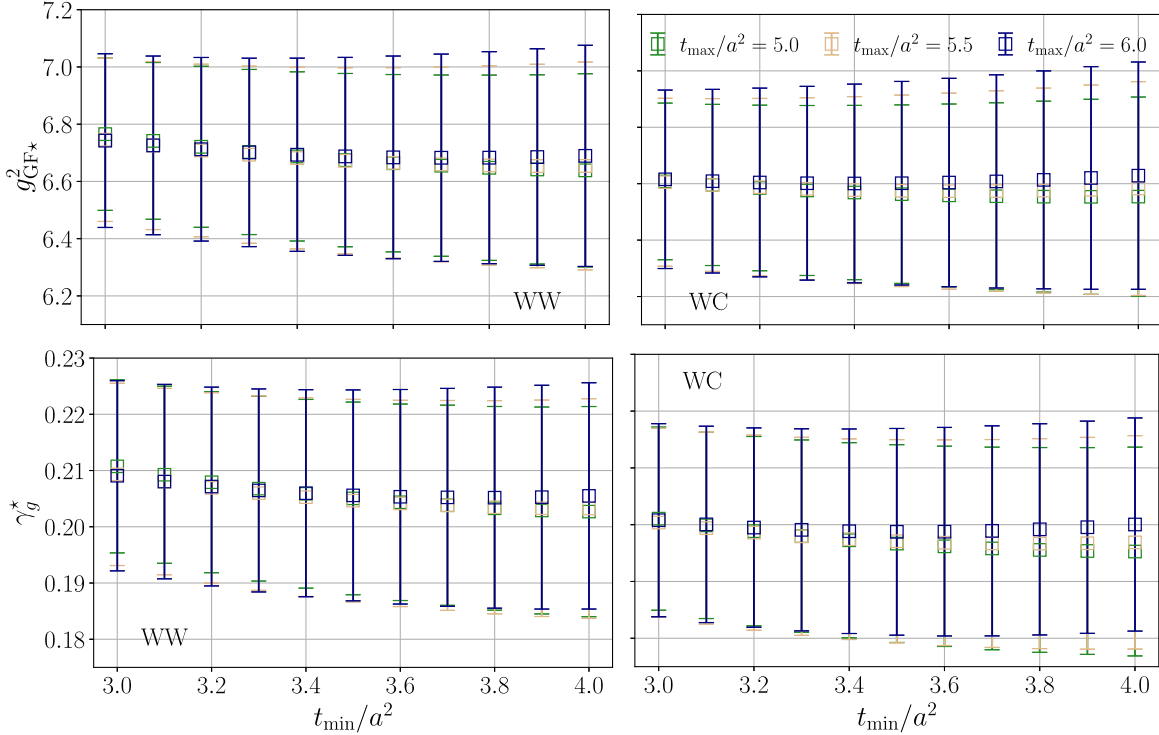


FIG. 8. Comparison of our estimated $g_{\text{GF}\star}^2$ and γ_g^* for different t_{min}/a^2 (x-axes) and $t_{\text{max}}/a^2 = 5.0$ (green), 5.5 (gold), 6.0 (navy) from the continuum extrapolation.

- (i) Choosing a higher-order polynomial for the intermediate interpolation in Sec. III B. The highest-order interpolation in N that we can use before we lose control over our continuum extrapolation due to overfitting is $N = 6$. This shifts the value of γ_g^* by ≈ 0.001 , and we take the latter difference as an estimate for the systematic error that is associated with our choice of N for the intermediate interpolation.
- (ii) Choosing a different $t_{\text{min}}/a^2, t_{\text{max}}/a^2$ in the continuum extrapolation. We estimate the systematic error that is associated with our choice of $t_{\text{min}}/a^2, t_{\text{max}}/a^2$ by the difference in the most extreme values of γ_g^* in our variations illustrated in Fig. 8. This yields a systematic error of ≈ 0.006 .
- (iii) Choosing instead the prediction for $\gamma_g^* = 0.206(19)$ from the WW combination as our central result. We take the difference in these predictions (≈ 0.007) as an estimate of the systematic error associated with making a particular choice of flow/operator combination.

To be conservative, we combine the error in our analysis of γ_g^* with the systematic error estimates above linearly. This yields the final prediction $\gamma_g^* = 0.199(32)$. Repeating the same exercise for $g_{\text{GF}\star}^2$ yields a systematic error of ≈ 0.12 from the interpolation order, ≈ 0.05 from the continuum extrapolation, and ≈ 0.09 from the flow/operator combination. Including the systematic error in $g_{\text{GF}\star}^2$ linearly yields a final prediction of $g_{\text{GF}\star}^2 = 6.60(62)$.

In Fig. 9 we compare our prediction for γ_g^* with those available in the literature [6,21]. Our result is plotted as a maroon star with errors indicated by an error bar. The smaller error bar is our error estimate before accounting for systematic effects and the larger error bar includes systematic effects. The result for γ_g^* from the perturbative calculation of Ref. [6] (dark gold error bar) is within 1σ of our estimate for γ_g^* . The lattice calculation of γ_g^* from Ref. [21] (cyan error bar) is within 2σ of our result.

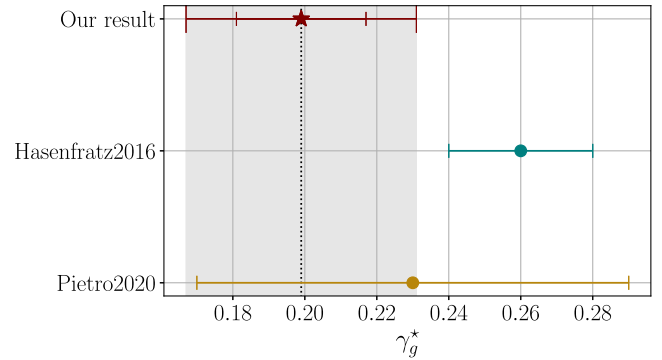


FIG. 9. Comparison of our value for γ_g^* (maroon error bar) against Ref. [21] (teal error bar) and Ref. [6] (dark gold error bar). The smaller error bar on our result indicates the error without accounting for systematic effects; the larger error bar indicates our error after accounting for systematic effects. We indicate our total error with a grey band for visualization.

However, it is important to note that the lattice calculation in Ref. [21] uses smaller volumes and very coarse lattices in comparison to the present work. It is also worth noting the “scheme-independent” prediction of $\gamma_g^* \approx 0.228$ from Ref. [4] is also within 1σ of our predicted γ_g^* ; we do not show this result in Fig. 9 because no estimate of the systematic error in this result is available.

V. CONCLUSIONS

We have calculated the non-perturbative β function of the SU(3) gauge-fermion system with twelve massless fundamental fermions using a Pauli-Villars improved lattice action. We find strong evidence for an infrared fixed point at $g_{\text{GF}^*}^2 = 6.60(62)$ from our gradient-flow-based renormalization scheme. Our study utilizes a wide range of couplings and volumes. In particular, we can reach renormalized gauge coupling values well above the predicted IRFP without the interference of a bulk phase transition. We include systematic effects from the infinite volume extrapolation directly into our analysis using Bayesian model averaging. Our data exhibit cutoff effects that are consistent with the leading $\mathcal{O}(a^2/t)$ form over a wide range t/a^2 . The consistency between the W and C operators further supports the leading order scaling behavior. We believe the improved scaling is due to the additional PV bosons that reduce cutoff effects. In contrast, we found significantly larger cutoff effects when we reanalyzed the data that were generated without PV fields and used in Ref. [21]. Our data are publicly available at Ref. [70].

Overall, the systematics of our continuum extrapolation are well controlled. Based on the continuum prediction for $\beta(g_{\text{GF}}^2)$ in g_{GF}^2 , we estimate the leading irrelevant critical exponent $\gamma_g^* = 0.199(32)$. This estimate includes conservative systematic errors from various choices in our analysis. Our result for γ_g^* agrees with Refs. [4,6] at the 1σ level and Ref. [21] at the 2σ level.

Our gradient flow data is publicly available at Ref. [70] and our final prediction for the continuum beta function is also provided as a supplementary ASCII file [81].

ACKNOWLEDGMENTS

Both authors acknowledge support by DOE Grant No. DE-SC0010005. This material is based upon work supported by the National Science Foundation Graduate Research Fellowship Program under Grant No. DGE 2040434. The research reported in this work made use of computing and long-term storage facilities of the USQCD Collaboration, which are funded by the Office of Science of the U.S. Department of Energy. This work utilized the Alpine high-performance computing resource at the University of Colorado Boulder. Alpine is jointly funded by the University of Colorado Boulder, the University of Colorado Anschutz, and Colorado State University. We thank James Osborn and Xiaoyong Jin for writing QEX and helping us develop our QEX-based hybrid Monte Carlo and gradient flow codes.

-
- [1] Thomas A. Ryttov and Robert Shrock, Higher-loop corrections to the infrared evolution of a gauge theory with fermions, *Phys. Rev. D* **83**, 056011 (2011).
 - [2] Claudio Pica and Francesco Sannino, UV and IR zeros of gauge theories at the four loop order and beyond, *Phys. Rev. D* **83**, 035013 (2011).
 - [3] Thomas A. Ryttov and Robert Shrock, Infrared zero of β and value of γ_m for an SU(3) gauge theory at the five-loop level, *Phys. Rev. D* **94**, 105015 (2016).
 - [4] Thomas A. Ryttov and Robert Shrock, Higher-order scheme-independent series expansions of $\gamma_{\bar{\psi}\psi,IR}$ and β'_{IR} in conformal field theories, *Phys. Rev. D* **95**, 105004 (2017).
 - [5] Thomas A. Ryttov and Robert Shrock, Scheme-independent series expansions at an infrared zero of the beta function in asymptotically free gauge theories, *Phys. Rev. D* **94**, 125005 (2016).
 - [6] Lorenzo Di Pietro and Marco Serone, Looking through the QCD conformal window with perturbation theory, *J. High Energy Phys.* **07** (2020) 049.
 - [7] Thomas Appelquist, Anuradha Ratnaweera, John Terning, and L. C. R. Wijewardhana, The phase structure of an SU(N) gauge theory with N(f) flavors, *Phys. Rev. D* **58**, 105017 (1998).
 - [8] A. Bashir, A. Raya, and J. Rodriguez-Quintero, QCD: Restoration of chiral symmetry and deconfinement for large N_f , *Phys. Rev. D* **88**, 054003 (2013).
 - [9] Jens Braun and Holger Gies, Chiral phase boundary of QCD at finite temperature, *J. High Energy Phys.* **06** (2006) 024.
 - [10] Jens Braun, Christian S. Fischer, and Holger Gies, Beyond Miransky scaling, *Phys. Rev. D* **84**, 034045 (2011).
 - [11] Jong-Wan Lee, Conformal window from conformal expansion, *Phys. Rev. D* **103**, 076006 (2021).
 - [12] Zhijin Li and David Poland, Searching for gauge theories with the conformal bootstrap, *J. High Energy Phys.* **03** (2021) 172.
 - [13] Seth Grable and Paul Romatschke, Elements of confinement for QCD with twelve massless quarks, [arXiv:2310.12203](https://arxiv.org/abs/2310.12203).
 - [14] Hee Sok Chung and Daniel Negradi, f_Q/m_Q and f_π/m_Q ratios and the conformal window, *Phys. Rev. D* **107**, 074039 (2023).

- [15] Paul Romatschke, An alternative to perturbative renormalization in 3 + 1 dimensional field theories, [arXiv:2401.06847](#).
- [16] Thomas Appelquist, George T. Fleming, and Ethan T. Neil, Lattice study of the conformal window in QCD-like theories, *Phys. Rev. Lett.* **100**, 171607 (2008).
- [17] Thomas Appelquist, George T. Fleming, and Ethan T. Neil, Lattice study of conformal behavior in SU(3) Yang-Mills theories, *Phys. Rev. D* **79**, 076010 (2009).
- [18] C. J. David Lin, Kenji Ogawa, Hiroshi Ohki, and Eigo Shintani, Lattice study of infrared behaviour in SU(3) gauge theory with twelve massless flavours, *J. High Energy Phys.* **08** (2012) 096.
- [19] C. J. David Lin, Kenji Ogawa, and Alberto Ramos, The Yang-Mills gradient flow and SU(3) gauge theory with 12 massless fundamental fermions in a colour-twisted box, *J. High Energy Phys.* **12** (2015) 103.
- [20] Zoltan Fodor, Kieran Holland, Julius Kuti, Santanu Mondal, Daniel Negradi, and Chik Him Wong, Fate of the conformal fixed point with twelve massless fermions and SU(3) gauge group, *Phys. Rev. D* **94**, 091501 (2016).
- [21] Anna Hasenfratz and David Schaich, Nonperturbative β function of twelve-flavor SU(3) gauge theory, *J. High Energy Phys.* **02** (2018) 132.
- [22] Zoltan Fodor, Kieran Holland, Julius Kuti, Daniel Negradi, and Chik Him Wong, The twelve-flavor β -function and dilaton tests of the sextet scalar, *EPJ Web Conf.* **175**, 08015 (2018).
- [23] Zoltan Fodor, Kieran Holland, Julius Kuti, Daniel Negradi, and Chik Him Wong, Extended investigation of the twelve-flavor β -function, *Phys. Lett. B* **779**, 230 (2018).
- [24] A. Hasenfratz, C. Rebbi, and O. Witzel, Nonperturbative determination of β functions for SU(3) gauge theories with 10 and 12 fundamental flavors using domain wall fermions, *Phys. Lett. B* **798**, 134937 (2019).
- [25] Anna Hasenfratz, Claudio Rebbi, and Oliver Witzel, Gradient flow step-scaling function for SU(3) with twelve flavors, *Phys. Rev. D* **100**, 114508 (2019).
- [26] Anna Hasenfratz, Conformal or walking? Monte Carlo renormalization group studies of SU(3) gauge models with fundamental fermions, *Phys. Rev. D* **82**, 014506 (2010).
- [27] Anna Hasenfratz, Infrared fixed point of the 12-fermion SU(3) gauge model based on 2-lattice MCRG matching, *Phys. Rev. Lett.* **108**, 061601 (2012).
- [28] Anna Hasenfratz and Oliver Witzel, Continuous β function for the SU(3) gauge systems with two and twelve fundamental flavors, *Proc. Sci. LATTICE2019* (**2019**) 094 [[arXiv:1911.11531](#)].
- [29] A. Deuzeman, M. P. Lombardo, and E. Pallante, Evidence for a conformal phase in SU(N) gauge theories, *Phys. Rev. D* **82**, 074503 (2010).
- [30] Zoltan Fodor, Kieran Holland, Julius Kuti, Daniel Negradi, and Chris Schroeder, Twelve massless flavors and three colors below the conformal window, *Phys. Lett. B* **703**, 348 (2011).
- [31] T. Appelquist, G. T. Fleming, M. F. Lin, E. T. Neil, and D. A. Schaich, Lattice simulations and infrared conformality, *Phys. Rev. D* **84**, 054501 (2011).
- [32] Thomas DeGrand, Finite-size scaling tests for spectra in SU(3) lattice gauge theory coupled to 12 fundamental flavor fermions, *Phys. Rev. D* **84**, 116901 (2011).
- [33] Zoltan Fodor, Kieran Holland, Julius Kuti, Daniel Negradi, Chris Schroeder, and Chik Him Wong, Conformal finite size scaling of twelve fermion flavors, *Proc. Sci. Lattice2012* (**2012**) 279.
- [34] Yasumichi Aoki, Tatsumi Aoyama, Masafumi Kurachi, Toshihide Maskawa, Kei-ichi Nagai, Hiroshi Ohki, Akihiro Shibata, Koichi Yamawaki, and Takeshi Yamazaki (LatKMI Collaboration), Lattice study of conformality in twelve-flavor QCD, *Phys. Rev. D* **86**, 054506 (2012).
- [35] Yasumichi Aoki, Tatsumi Aoyama, Masafumi Kurachi, Toshihide Maskawa, Kei-ichi Nagai, Hiroshi Ohki, Enrico Rinaldi, Akihiro Shibata, Koichi Yamawaki, and Takeshi Yamazaki (LatKMI Collaboration), Light composite scalar in twelve-flavor QCD on the lattice, *Phys. Rev. Lett.* **111**, 162001 (2013).
- [36] Anqi Cheng, Anna Hasenfratz, Yuzhi Liu, Gregory Petropoulos, and David Schaich, Finite size scaling of conformal theories in the presence of a near-marginal operator, *Phys. Rev. D* **90**, 014509 (2014).
- [37] M. P. Lombardo, K. Miura, T. J. Nunes da Silva, and E. Pallante, On the particle spectrum and the conformal window, *J. High Energy Phys.* **12** (2014) 183.
- [38] Zoltan Fodor, Kieran Holland, Julius Kuti, Daniel Negradi, and Chris Schroeder, Nearly conformal gauge theories in finite volume, *Phys. Lett. B* **681**, 353 (2009).
- [39] Anqi Cheng, Anna Hasenfratz, Gregory Petropoulos, and David Schaich, Scale-dependent mass anomalous dimension from Dirac eigenmodes, *J. High Energy Phys.* **07** (2013) 061.
- [40] Zoltan Fodor, Kieran Holland, Julius Kuti, Daniel Negradi, and Chik Him Wong, Case studies of near-conformal β -functions, *Proc. Sci. LATTICE2019* (**2019**) 121 [[arXiv:1912.07653](#)].
- [41] Albert Deuzeman, Maria Paola Lombardo, Tiago Nunes Da Silva, and Elisabetta Pallante, The bulk transition of QCD with twelve flavors and the role of improvement, *Phys. Lett. B* **720**, 358 (2013).
- [42] Tiago Nunes da Silva and Elisabetta Pallante, The strong coupling regime of twelve flavors QCD, *Proc. Sci. LATTICE2012* (**2012**) 052 [[arXiv:1211.3656](#)].
- [43] David Schaich, Anqi Cheng, Anna Hasenfratz, and Gregory Petropoulos, Bulk and finite-temperature transitions in SU(3) gauge theories with many light fermions, *Proc. Sci. LATTICE2012* (**2012**) 028 [[arXiv:1207.7164](#)].
- [44] Tobias Rindlisbacher, Kari Rummukainen, and Ahmed Salami, Bulk-preventing actions for SU(N) gauge theories, *Proc. Sci. LATTICE2021* (**2022**) 576 [[arXiv:2111.00860](#)].
- [45] Tobias Rindlisbacher, Kari Rummukainen, and Ahmed Salami, Bulk-transition-preventing actions for SU(N) gauge theories, *Phys. Rev. D* **108**, 114511 (2023).
- [46] Felix Springer, David Schaich, and Enrico Rinaldi (Lattice Strong Dynamics (LSD) Collaboration), First-order bulk transitions in large- N lattice Yang–Mills theories using the density of states, [arXiv:2311.10243](#).

- [47] Anna Hasenfratz, Yigal Shamir, and Benjamin Svetitsky, Taming lattice artifacts with Pauli-Villars fields, *Phys. Rev. D* **104**, 074509 (2021).
- [48] Anna Hasenfratz, Ethan T. Neil, Yigal Shamir, Benjamin Svetitsky, and Oliver Witzel, Infrared fixed point and anomalous dimensions in a composite Higgs model, *Phys. Rev. D* **107**, 114504 (2023).
- [49] Anna Hasenfratz, Ethan T. Neil, Yigal Shamir, Benjamin Svetitsky, and Oliver Witzel, Infrared fixed point of the SU(3) gauge theory with $N_f = 10$ flavors, *Phys. Rev. D* **108**, L071503 (2023).
- [50] R. Narayanan and H. Neuberger, Infinite N phase transitions in continuum Wilson loop operators, *J. High Energy Phys.* **03** (2006) 064.
- [51] Martin Lüscher, Trivializing maps, the Wilson flow and the HMC algorithm, *Commun. Math. Phys.* **293**, 899 (2010).
- [52] Martin Lüscher, Properties and uses of the Wilson flow in lattice QCD, *J. High Energy Phys.* **08** (2010) 071.
- [53] Zoltan Fodor, Kieran Holland, Julius Kuti, Daniel Nogradi, and Chik Him Wong, A new method for the β function in the chiral symmetry broken phase, *EPJ Web Conf.* **175**, 08027 (2018).
- [54] Andrea Carosso, Anna Hasenfratz, and Ethan T. Neil, Nonperturbative renormalization of operators in near-conformal systems using gradient flows, *Phys. Rev. Lett.* **121**, 201601 (2018).
- [55] Andrea Carosso, Stochastic renormalization group and gradient flow, *J. High Energy Phys.* **01** (2020) 172.
- [56] Anna Hasenfratz and Oliver Witzel, Continuous renormalization group β function from lattice simulations, *Phys. Rev. D* **101**, 034514 (2020).
- [57] Anna Hasenfratz, Christopher J. Monahan, Matthew David Rizik, Andrea Shindler, and Oliver Witzel, A novel non-perturbative renormalization scheme for local operators, *Proc. Sci. LATTICE2021* (2022) 155 [arXiv:2201.09740].
- [58] Robert V. Harlander and Tobias Neumann, The perturbative QCD gradient flow to three loops, *J. High Energy Phys.* **06** (2016) 161.
- [59] Daniel Nogradi and Agostino Patella, Strong dynamics, composite Higgs and the conformal window, *Int. J. Mod. Phys. A* **31**, 1643003 (2016).
- [60] Hiroki Makino, Okuto Morikawa, and Hiroshi Suzuki, Gradient flow and the Wilsonian renormalization group flow, *Prog. Theor. Exp. Phys.* **2018**, 053B02 (2018).
- [61] Julius Kuti, Zoltán Fodor, Kieran Holland, and Chik Him Wong, From ten-flavor tests of the β -function to α_s at the Z-pole, *Proc. Sci. LATTICE2021* (2022) 321 [arXiv:2203.15847].
- [62] Anna Hasenfratz, Curtis Taylor Peterson, Jake van Sickle, and Oliver Witzel, Λ parameter of the SU(3) Yang-Mills theory from the continuous β function, *Phys. Rev. D* **108**, 014502 (2023).
- [63] Chik Him Wong, Szabolcs Borsanyi, Zoltan Fodor, Kieran Holland, and Julius Kuti, Toward a novel determination of the strong QCD coupling at the Z-pole, *Proc. Sci. LATTICE2022* (2023) 043.
- [64] Curtis T. Peterson, Anna Hasenfratz, Jake van Sickle, and Oliver Witzel, Determination of the continuous β function of SU(3) Yang-Mills theory, *Proc. Sci. LATTICE2021* (2022) 174.
- [65] Anna Hasenfratz and Francesco Knechtli, Flavor symmetry and the static potential with hypercubic blocking, *Phys. Rev. D* **64**, 034504 (2001).
- [66] Anna Hasenfratz, Roland Hoffmann, and Stefan Schaefer, Hypercubic smeared links for dynamical fermions, *J. High Energy Phys.* **05** (2007) 029.
- [67] Anqi Cheng, Anna Hasenfratz, and David Schaich, Novel phase in SU(3) lattice gauge theory with 12 light fermions, *Phys. Rev. D* **85**, 094509 (2012).
- [68] S. Duane, A. D. Kennedy, B. J. Pendleton, and D. Roweth, Hybrid Monte Carlo, *Phys. Lett. B* **195**, 216 (1987).
- [69] J. Osborn and Xiao-Yong Jin, Introduction to the Quantum EXpressions (QEX) framework, *Proc. Sci. LATTICE2016* (2017) 271.
- [70] Curtis Peterson and Anna Hasenfratz, Twelve flavor SU(3) gradient flow data for the continuous beta-function (Zenodo, 2024), [10.5281/zenodo.10719052](https://doi.org/10.5281/zenodo.10719052).
- [71] Ulli Wolff (ALPHA Collaboration), Monte Carlo errors with less errors, *Comput. Phys. Commun.* **156**, 143 (2004).
- [72] Stefan Schaefer, Rainer Sommer, and Francesco Virota (ALPHA Collaboration), Critical slowing down and error analysis in lattice QCD simulations, *Nucl. Phys.* **B845**, 93 (2011).
- [73] Alberto Ramos, Automatic differentiation for error analysis, *Proc. Sci. TOOLS2020* (2021) 045 [arXiv:2012.11183].
- [74] Fabian Joswig, Simon Kuberski, Justus T. Kuhlmann, and Jan Neuendorf, PYERRORS: A Python framework for error analysis of Monte Carlo data, *Comput. Phys. Commun.* **288**, 108750 (2023).
- [75] Zoltan Fodor, Kieran Holland, Julius Kuti, Daniel Nogradi, and Chik Him Wong, The Yang-Mills gradient flow in finite volume, *J. High Energy Phys.* **11** (2012) 007.
- [76] Peter Lepage, gvar (2015).
- [77] Curtis Peterson, SwissFit, <https://github.com/ctpeterson/SwissFit>.
- [78] William I. Jay and Ethan T. Neil, Bayesian model averaging for analysis of lattice field theory results, *Phys. Rev. D* **103**, 114502 (2021).
- [79] Ethan T. Neil and Jacob W. Sitison, Improved information criteria for Bayesian model averaging in lattice field theory, *Phys. Rev. D* **109**, 014510 (2024).
- [80] Ethan T. Neil and Jacob W. Sitison, Model averaging approaches to data subset selection, *Phys. Rev. E* **108**, 045308 (2023).
- [81] See Supplemental Material at <http://link.aps.org/supplemental/10.1103/PhysRevD.109.114507> for our final result of the continuous beta function in the form of an ASCII file.